Experimental Insights into LQR-Controlled Penta Copter Blimps: Design, Construction and Output Evaluation

Md. Tasnim Rana[1*], Md Miraj Arefin[2], Hosney Ara[1], Md. Shahidul Islam[2]

[1] Bangladesh Council of Scientific and Industrial Research (BCSIR), Bangladesh

[2] Khulna University of Engineering & Technology (KUET), Khulna, Bangladesh

Abstract:

This study presents a comprehensive analysis of the design, construction, and control of a Lighter-Than-Air (LTA) penta copter blimp, focusing on enhanced performance through dynamic modeling, propulsion system optimization, and the application of a Linear Quadratic Regulator (LQR)-based control system. The drone's equations of motion are thoroughly examined in the dynamic modeling portion, which also takes buoyancy and aerodynamic forces into account to precisely represent the drone's behavior in a range of operating circumstances. The propulsion system analysis is concerned with determining the critical characteristics that impact the efficiency of the selected propulsion system and modeling techniques for it. The integration of an LQR-based control system is examined, emphasizing the benefits and guiding principles of using it with aerial drones. Through MATLAB simulations and subsequent real-world experiments, the synergistic effects of the propulsion system, dynamic modeling, and LQR control are evaluated. The findings highlight the importance of this integrated approach in expanding the capabilities of aerial drone technology and provide useful information for maximizing design considerations and operational capabilities.

Keywords: Lighter-than-air, Dynamic Modeling, Propulsion system, LQR-based control, Optimization

*Corresponding author: rana.me.kuet@gmail.com (Md. Tasnim Rana)

Nomenclature

m	Mass	R	Transformation matrix
F_1, F_2, F_3, F_4, F_5	Force of the thrusters	R	Reference Input
x, y, z	Position along x, y, z axis	K	LQR gain vector
$\dot{x}, \dot{y}, \dot{z}$	Velocity along x, y, z axis	ω	Angular velocity
$\ddot{x}, \ddot{y}, \ddot{z}$	Acceleration along x, y, z axis	F_D	Drag Force
φ, θ, ψ	Roll, Pitch, Yaw angle	g	Acceleration due to gravity
$\dot{\varphi}, \dot{\theta}, \dot{\psi}$	Roll, Pitch, Yaw angular velocity	$\dot{e}$	Integral gain
$\ddot{\varphi}, \ddot{\theta}, \ddot{\psi}$	Roll, Pitch, Yaw angular acceleration	*Abbreviation*	
A	System matrix	LQR	Linear Quadratic Regulator

B	Input matrix	LTA	Lighter Than Air
C	Output matrix	BLDC	Brushless Direct Current
D	Feed forward matrix	UAV	Unmanned Aerial Vehicle
$x(t)$	State Vector	GPS	Global Positioning System
$y(t)$	Output Vector	TG/DTA	Thermogravimetry/Differential Thermal Analysis
$u(t)$	Input Vector	DTG	Differential Thermogravimetric
$\Delta\rho$	Density difference	LIDAR	Light Detection and Ranging
I_x, I_y, I_z	Inertia along x, y, z axis	PID	Proportional-Integral-Derivative
k	Propeller constant	CG	Center of Gravity
V	Volume	CB	Center of Buoyancy
S	Surface area	UV	Ultra Violet

1.0 Introduction

Aerial robotics has been a key area of research and development. Aerial robotics are used for a variety of purposes, including surveying and photography, defense operations, long-term observation or monitoring, border patrols, agricultural application, and so on. The primary research focus in aerial robots or drones is to increase the system's in-flight endurance and stability under any unfavorable conditions. Aerodynamic and battery enhancement research is being conducted in order to increase flying duration. However, a big airship without a hard body known as a blimp opened up a new avenue for academics to put old technologies into a new form. Blimp is primarily a non-rigid inflated envelope designed with aerodynamic considerations in mind. Its aerodynamic form is generated by its internal LTA gasses. Blimp features a confined chamber that retains LTA gases and generates buoyant forces owing to density differences. LTA gases are light in weight; hence they have a lower density at the same volume than ambient air. This density differential generates buoyancy force and provides lift to the blimp body. Without the control thrust, there is no need for extra lift force. So, for the same cargo capacity, the blimp needs less battery power, resulting in a longer flying period.

Over the years, the exploration of dynamic modeling, testing, and stability analysis within the domain of LTA vehicles, particularly automatic controlled blimps, and unmanned autonomous blimps, has evolved, showcasing a progression of research and advancements. The timeline begins with Herman et al.'s (2011) work [1], where a dynamic model effectively captures the nonlinear behavior of an ornithopter blimp near steady-state velocity. This early study lays the foundation for understanding the intricate dynamics of such aerial vehicles. In 2002, Yamasaki et al.[2] initiate identification of blimp dynamics through indoor free flight tests, setting the stage for experimental approaches in understanding these vehicles. The study suggests analytical formulas for parameter estimation, hinting at the potential integration of theoretical models with practical experiments.

The subsequent years witness an increasing focus on control mechanisms. Abdul Kadir et al. (2012) [3] emphasizes controllability through the implementation of optimal controllers,

addressing lateral model navigation issues in Upstate Research Rocketry Group (URRG) mono-hull blimps. The significance of stability and controllability, attributed to drag and buoyancy forces, becomes apparent, indicating a maturation in the field's understanding [4]. By 2005, Bestaoui's work contributes dynamic modeling using the Newton-Euler approach, marking a shift towards more sophisticated modeling techniques [5]. The study presents a dynamic modeling approach for autonomous blimps, shedding light on their motion in six degrees of freedom. Advancements in control systems continue to emerge. Kawai et al. (2003) propose a visual feedback control mechanism for an unmanned planar blimp, designing a linearizing feedback PD controller for trajectory tracking [6]. This period witnesses the integration of visual feedback systems into blimp control strategies. In 2006, Zufferey's research introduces neuromorphic controllers evolved through simulation for steering indoor airships. This marks a departure from traditional control approaches, with an emphasis on artificial neural networks and physics-based dynamic modeling [7].

The timeline progresses to 2014, where Song et al. design a PID controller for disturbance handling during autonomous flight, showcasing the growing sophistication of control strategies [8]. The efficacy of the PID controller is demonstrated through simulation results, providing a glimpse into the potential for autonomous blimp control systems [9]. Van Asares et al.'s work in 2018 represents a contemporary application of blimp technology [10]. The design of an unmanned aerial vehicle blimp capable of successful flight and maneuverability in confined indoor spaces reflects recent advancements in material selection, profile making, microcontroller programming, and flight testing.

In conclusion, the timeline reflects the chronological evolution of research in dynamic modeling, testing, and stability analysis of blimps, from early investigations into their nonlinear behavior to the contemporary design and testing of advanced Unmanned Aerial Vehicle (UAV) blimps. This progression underscores the continuous development of knowledge and technology in this field. Most of the modeling has been done with PD or PID or other kind of control system. Along with this situation, traditional propulsion system has specific trust point for giving the blimp a mobility. So, most of the state space equation has the same point node as control parameters. There are a lot of control system in aerial control dynamics. But very few works have been done on LQR based controller.

This paper discusses the modeling and control of a LTA Aerial Drone, which has five propellers and five BLDC motors which has a new propulsion dynamic. This new dynamic system results in new state space equation which would make the control system with in a close loop while functioning. Normal quadcopter is an under-actuated system with six degrees of freedom and rotation of propellers generates upward thrust forces. Common control strategies for quadcopters include proportional-derivative PD, proportional-integral-derivative PID, LQR, and Fuzzy [11]. LQR is widely used control system that not only deals with fast response but also control over the energy consumption upon the system propulsion system. LQR provides optimal control, minimizing a quadratic cost function [12]. This paper applies LQR based control on positions and yaw orientation of the quadcopter, performing simulations to observe control performance.

Integral feedback is applied on altitude to improve response while considering a fifth propulsion system and a nontraditional LTA vehicle platform. Previously a lot of work has been done regarding various control system with quadrotor but this research work deals with a Penta copter configuration. The base system is not a traditional UAV for the primary lifting it works with the LTA gasses. The main focus was that; LTA system is mainly used for long time flight capability. Most of the case the system is controlled by manual control system. But this paper work dealt with a Penta copter control system for this LTA based Blimp while considering LQR. As, the main focus for using LTA system is to make the aerial vehicle keep longer on the air but PID or other control system can only deal with the time dependent stability [13]. As the main focus of stablishing a system for long duration flight, instead of using PID, PD or other related control system, LQR based control system has been introduced for proper energy management. Moreover, LQR with integral term could help reduce steady state error in the complex 3-D space motion of the quadcopter.

2.0 Propulsion System Modeling

Any kind of system get momentum through some force providing accusation system. In case of aerodynamic system, rotating fuel engine or electrical motor has been used for generating thrust through the rotational propeller designed for specific aerodynamic modeling. In the study, we've used Penta-copter concept where brushless DC motor in short BLDC motor has been used. As the control system operates in a closed loop, it requires force balance within the propulsion system to function effectively. So, both the traditional and proposed Penta-copter model has been introduced for signifying the similarity and novelty of the proposed system.

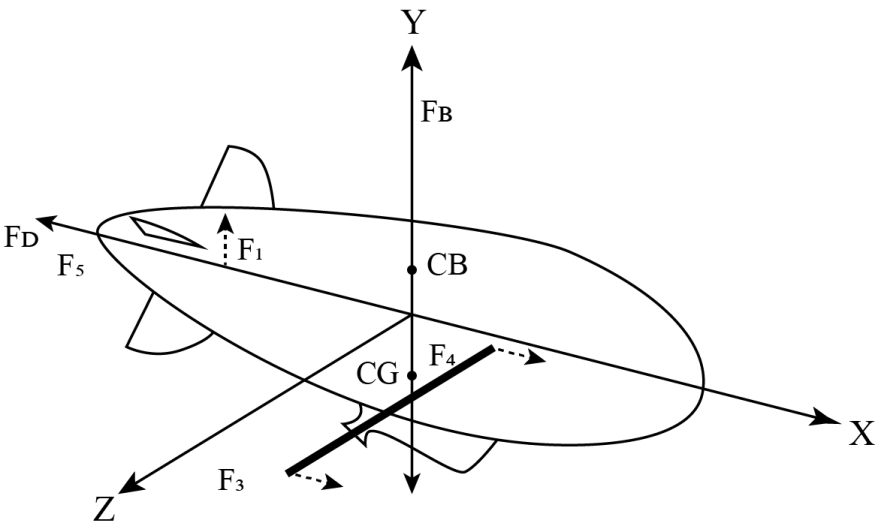

(a)

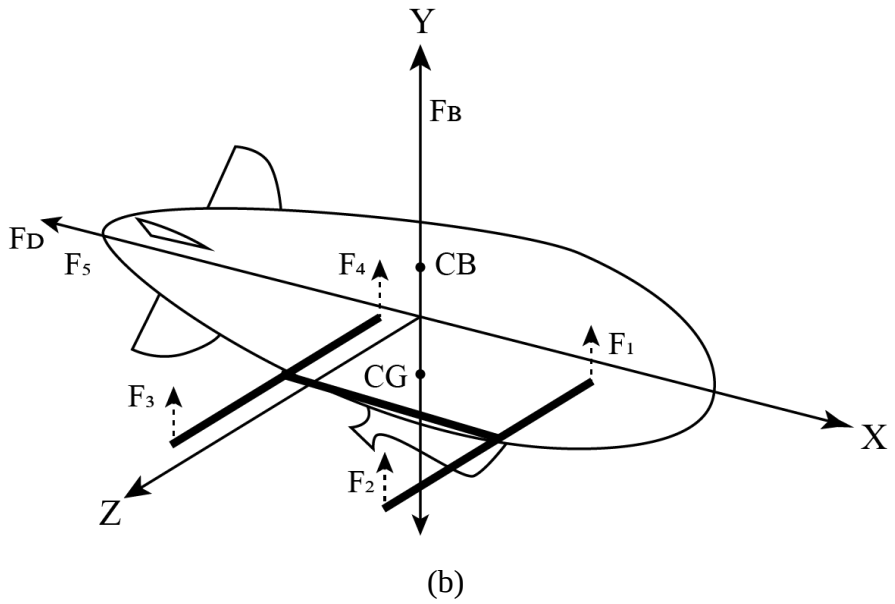

(b)

Fig. 1. Dynamic Modeling of the LTA blimp (a) Traditional blimp control (b) Penta copter blimp control

In the Fig. 1(a), a model blimp has been shown. Traditional work related to blimp has two or three propulsion or control output. Where F1, F3, F4 worked as a propulsion system and by rotating the thrust direction the system would gain its mobility. For forward direction movement, the propulsion system of F3 and F4 would rotate at 90 degrees and would gain its forward moving propulsion. For left and right movement, the angular propulsion control of F1 would create a thrust force. Most of the traditional Blimp or airship propulsion system does not have five propulsion system. In figure 1-b, a proposed Penta-copter model has been introduced. But the proposed propulsion system is also used in vertical takeoff and landing systems known as VTOL. But the novelty of the proposed system is that, it has been introduced in a LTA system. LTA gas mainly deals with the lifting force and additional 5 BLDC motor would work as the main thrust generating unit. In the Fig. 1(b) total five propulsion system has been shown F1, F2, F3, F4, F5. F1-4 is mainly responsible for stabilizing and balancing the blimp and F5 is mainly responsible for providing the forward thrust.

As the system in Fig. 1. is in a fixed frame which is represented by x-y-z, where the inertial frame is represented as X-Y-Z. The transformation between these two frames is expressed in the following transformation matrix R. Which is obtained by the Euler angles (φ, θ, and ψ) about x, y and z axis.

$$[R] = \begin{bmatrix} c\theta c\psi & s\phi s\theta c\psi - c\phi s\psi & c\psi s\theta c\phi + s\phi s\psi \\ c\theta s\psi & s\phi s\theta s\psi - c\phi s\psi & c\psi s\theta s\phi - s\phi s\psi \\ -s\theta & s\phi c\theta & c\phi c\theta \end{bmatrix}$$

Here, $c\theta = \cos(\theta)$ and $s\theta = \sin(\theta)$

3.0 System Dynamics

As the Newton's equation:

$$m\begin{bmatrix}\ddot{x}\\ \ddot{y}\\ \ddot{z}\end{bmatrix}=[R]\begin{bmatrix}0\\ 0\\ F_1+F_2+F_3+F_4\end{bmatrix}+\begin{bmatrix}-F_d\\ 0\\ -mg+\Delta\rho gv\end{bmatrix}+\begin{bmatrix}F_5\\ 0\\ 0\end{bmatrix} \tag{1}$$

Here, m is the total mass received from cancelling out bouncy force, F_1, F_2, F_3, F_4 are the thrust force from the motor propeller generated by BLDC motor controlled with electric speed controller. F_5 is the thruster along the x axis for additional velocity in the direction of x just like a fixed wing thruster. R is the transformation matrix and $\Delta\rho gv$ is the bouncy force dependent on the altitude and which LTA gas is being used with quality. Though, during the calculation, the variation of bouncy force along with the variation of height is neglected.

$$m=\frac{(Mg-\Delta\rho vg)}{g}=M+\Delta\rho gv \tag{2}$$

Here $\Delta\rho$ is the difference in density between air and LTA gas. As the additional thruster F_5 works along x axis, it would work in the opposite direction of Drag force.

3.1 Nonlinear form of dynamic equations

From the transfer matrix and Newton's equation, the following equation are obtained.

$$\ddot{x}=\frac{(F_1+F_2+F_3+F_4)}{m}(-\theta)+\frac{F_5}{m}=-g\theta+\frac{F_5}{m} \tag{3}$$

$$\ddot{y}=g\varphi \tag{4}$$

$$\ddot{z}=\frac{(F_1+F_2+F_3+F_4)}{m} \tag{5}$$

$$\ddot{\phi}=(\frac{l}{I_x}F_1+\frac{l}{I_x}F_2-\frac{l}{I_x}F_3-\frac{l}{I_x}F_4)+\ddot{\theta}\ddot{\psi}(I_y-I_z) \tag{6}$$

$$\ddot{\theta}=(\frac{l}{I_y}F_1+\frac{l}{I_y}F_4-\frac{l}{I_y}F_2-\frac{l}{I_y}F_3)+\ddot{\phi}\ddot{\psi}(I_x-I_z) \tag{7}$$

$$\ddot{\psi}=(\frac{l}{I_z}F_1+\frac{l}{I_z}F_3-\frac{l}{I_z}F_2-\frac{l}{I_z}F_4)+\ddot{\phi}\ddot{\theta}(I_y-I_x) \tag{8}$$

3.2 Linear Form of the equations

By forming a linear format of the above equations, the model is linearized about the equilibrium hovering point, and the linear system of equation is given as follows.

$$\ddot{x} = -g\theta + \frac{1}{m}F_5 \tag{9}$$

$$\ddot{y} = g\varphi \tag{10}$$

$$\ddot{z} = \frac{1}{m}F_1 + \frac{1}{m}F_2 + \frac{1}{m}F_3 + \frac{1}{m}F_4 \tag{11}$$

$$\ddot{\phi} = (\frac{l}{I_x}F_1 + \frac{l}{I_x}F_2 - \frac{l}{I_x}F_3 - \frac{l}{I_x}F_4) \tag{12}$$

$$\ddot{\theta} = (\frac{l}{I_y}F_1 + \frac{l}{I_y}F_4 - \frac{l}{I_y}F_2 - \frac{l}{I_y}F_3) \tag{13}$$

$$\ddot{\psi} = (\frac{l}{I_z}F_1 + \frac{l}{I_z}F_3 - \frac{l}{I_z}F_2 - \frac{l}{I_z}F_4) \tag{14}$$

From equation 9 to 14 we would have the value for the state space equation 15.

$$\dot{x}_v = Ax_v + Bu \tag{15}$$

Using the equations from equation no 9 to 14 and using them in equation no 15, we have the following matrix equation

$$\begin{bmatrix} \dot{x} \\ \dot{y} \\ \dot{z} \\ \ddot{x} \\ \ddot{y} \\ \ddot{z} \\ \dot{\phi} \\ \dot{\theta} \\ \dot{\psi} \\ \ddot{\phi} \\ \ddot{\theta} \\ \ddot{\psi} \end{bmatrix} = \begin{bmatrix} 0 & 0 & 0 & 1 & 0 & 0 & 0 & 0 & 0 & 0 & 0 & 0 \\ 0 & 0 & 0 & 0 & 1 & 0 & 0 & 0 & 0 & 0 & 0 & 0 \\ 0 & 0 & 0 & 0 & 0 & 1 & 0 & 0 & 0 & 0 & 0 & 0 \\ 0 & 0 & 0 & 0 & 0 & 0 & 0 & -g & 0 & 0 & 0 & 0 \\ 0 & 0 & 0 & 0 & 0 & 0 & g & 0 & 0 & 0 & 0 & 0 \\ 0 & 0 & 0 & 0 & 0 & 0 & 0 & 0 & 0 & 0 & 0 & 0 \\ 0 & 0 & 0 & 0 & 0 & 0 & 0 & 0 & 0 & 1 & 0 & 0 \\ 0 & 0 & 0 & 0 & 0 & 0 & 0 & 0 & 0 & 0 & 1 & 0 \\ 0 & 0 & 0 & 0 & 0 & 0 & 0 & 0 & 0 & 0 & 0 & 1 \\ 0 & 0 & 0 & 0 & 0 & 0 & 0 & 0 & 0 & 0 & 0 & 0 \\ 0 & 0 & 0 & 0 & 0 & 0 & 0 & 0 & 0 & 0 & 0 & 0 \\ 0 & 0 & 0 & 0 & 0 & 0 & 0 & 0 & 0 & 0 & 0 & 0 \end{bmatrix} \begin{bmatrix} x \\ y \\ z \\ \dot{x} \\ \dot{y} \\ \dot{z} \\ \phi \\ \theta \\ \psi \\ \dot{\phi} \\ \dot{\theta} \\ \dot{\psi} \end{bmatrix} + \begin{bmatrix} 0 & 0 & 0 & 0 & 0 \\ 0 & 0 & 0 & 0 & 0 \\ 0 & 0 & 0 & 0 & 0 \\ 0 & 0 & 0 & 0 & \frac{1}{m} \\ 0 & 0 & 0 & 0 & 0 \\ \frac{1}{m} & \frac{1}{m} & \frac{1}{m} & \frac{1}{m} & 0 \\ 0 & 0 & 0 & 0 & 0 \\ 0 & 0 & 0 & 0 & 0 \\ 0 & 0 & 0 & 0 & 0 \\ \frac{l}{I_x} & \frac{l}{I_x} & -\frac{l}{I_x} & -\frac{l}{I_x} & 0 \\ \frac{l}{I_y} & -\frac{l}{I_y} & -\frac{l}{I_y} & \frac{l}{I_y} & 0 \\ \frac{l}{I_z} & -\frac{l}{I_z} & \frac{l}{I_z} & -\frac{l}{I_z} & 0 \end{bmatrix} \begin{bmatrix} F_1 \\ F_2 \\ F_3 \\ F_4 \\ F_5 \end{bmatrix} \tag{16}$$

Where,

$$A=\begin{bmatrix}0&0&0&1&0&0&0&0&0&0&0&0\\0&0&0&0&1&0&0&0&0&0&0&0\\0&0&0&0&0&1&0&0&0&0&0&0\\0&0&0&0&0&0&0&-g&0&0&0&0\\0&0&0&0&0&0&g&0&0&0&0&0\\0&0&0&0&0&0&0&0&0&0&0&0\\0&0&0&0&0&0&0&0&0&1&0&0\\0&0&0&0&0&0&0&0&0&0&1&0\\0&0&0&0&0&0&0&0&0&0&0&1\\0&0&0&0&0&0&0&0&0&0&0&0\\0&0&0&0&0&0&0&0&0&0&0&0\\0&0&0&0&0&0&0&0&0&0&0&0\end{bmatrix} \tag{17}$$

$$B=\begin{bmatrix}0&0&0&0&0\\0&0&0&0&0\\0&0&0&0&0\\0&0&0&0&\frac{1}{m}\\0&0&0&0&0\\\frac{1}{m}&\frac{1}{m}&\frac{1}{m}&\frac{1}{m}&0\\0&0&0&0&0\\0&0&0&0&0\\0&0&0&0&0\\\frac{l}{I_x}&\frac{l}{I_x}&-\frac{l}{I_x}&-\frac{l}{I_x}&0\\\frac{l}{I_y}&-\frac{l}{I_y}&-\frac{l}{I_y}&\frac{l}{I_y}&0\\\frac{l}{I_z}&-\frac{l}{I_z}&\frac{l}{I_z}&-\frac{l}{I_z}&0\end{bmatrix} \tag{18}$$

$$C=\begin{bmatrix}1&0&0&0&0&0&0&0&0&0&0&0\\0&1&0&0&0&0&0&0&0&0&0&0\\0&0&1&0&0&0&0&0&0&0&0&0\\0&0&0&0&0&0&1&0&0&0&0&0\\0&0&0&0&0&0&0&1&0&0&0&0\\0&0&0&0&0&0&0&0&1&0&0&0\end{bmatrix} \tag{19}$$

$$D=\begin{bmatrix}0&0&0&0&0\\0&0&0&0&0\\0&0&0&0&0\\0&0&0&0&0\\0&0&0&0&0\\0&0&0&0&0\end{bmatrix} \tag{20}$$

$$F_i=k_i\omega_i^2 \tag{21}$$

4.0 System Control

LQR is an optimal control method depicted in Fig. 2. wherein the objective is to minimize a quadratic cost function, J.

$$J = \int_0^\infty (x_v^T Q x_v + u^T R u) dt \tag{22}$$

In this context, Q (size $n \times n$, where n represents the number of states) and R (size $m \times m$, where m represents the number of inputs) denote positive definite symmetric matrices.

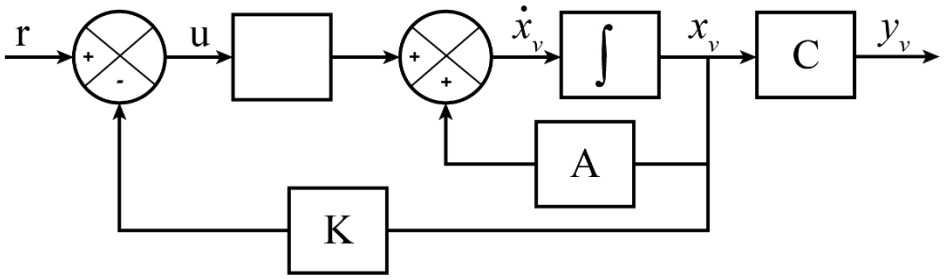

Fig. 2. LQR control diagram.

$$u = -K x_v + r \tag{23}$$

Where, u is the control input and r is the reference input, and the LQR gain vector K is represented as:

$$K = R^{-1} B^T P \tag{24}$$

Where, P is a positive definite symmetric constant matrix. P is obtained from the Reccati equation as given below.

$$A^T P + PA - PBR^{(-1)} B^T P + Q = 0 \tag{24}$$

Matrices Q and R are taken as follows: $Q = diag\left([1,\ 1,\ 1,\ 0,\ 0,\ 0,\ 1,\ 1,\ 1,\ 0,\ 0,\ 0]\right)$ and $R = diag\left([1,\ 1,\ 1,\ 1,\ 1]\right)$.

Additionally, integral feedback can be incorporated into LQR to enhance control performance by reducing steady-state error. The integration of integral feedback into LQR is illustrated in Fig. 3 first

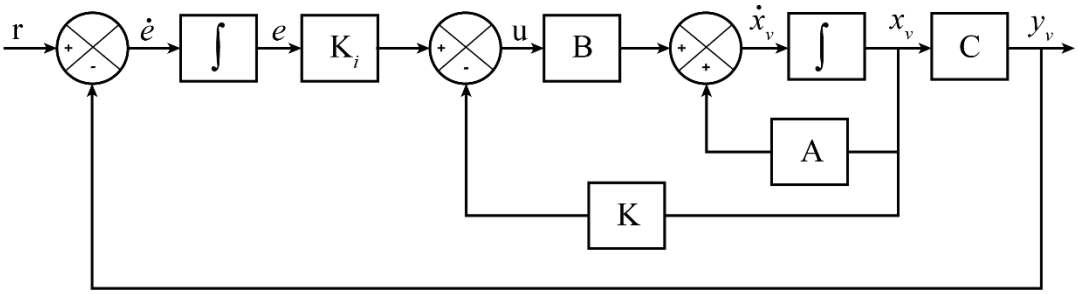

Fig. 3. LQR control with integral feedback.

The controlled input is given by:

$$u = -Kx_v + K_i e \tag{25}$$

Where, $\dot{e} = r - y_v$ and K_i represents the integral gain.

5.0 Design and fabrication of the blimp body

The Gertler 4154 series shape was chosen for designing the blimp due to its streamlined characteristics, initially developed by Israel Gertler and published in 1950 for high-speed submarine resistance experiments. This design later gained popularity in the LTA field, including airships. Modern non-rigid airships, commonly known as blimps, are now utilized as aerial robots or drones. This study primarily investigates how traditional control systems interact with LTA technologies.

For simplified mathematical calculations, the Gertler 4154 series shape was used for experimental purposes. The design is segmented into two parts, as shown in Fig. 4, forming the overall shape of the blimp, which acts as an aerodynamic streamliner during operation. Since the buoyancy force generated by LTA gas depends on the internal volume of the blimp, accurately calculating the envelope's volume is essential. When fully inflated, the volume of the LTA gas matches the envelope's total volume due to the absence of solid structures. The surface area of the envelope is also critical as it is used to determine aerodynamic friction, known as drag force. The calculations for both the volume and surface area of the envelope are presented in Table 1.

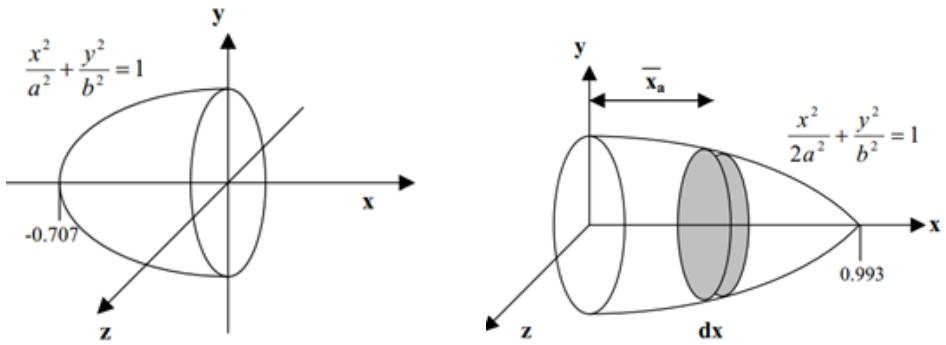

Fig. 4. Classical Gertler 4154 series shape for the blimp envelope

Table 1: Governing Equation for calculating the volume and surface area of the envelope

For Volume Measurements	For area Measurements
$V_1 = \pi \int_0^a b^2 - \frac{x^2 b^2}{a^2} dx = \frac{2}{3}\pi ab^2$	$S_1 = \int_0^a 2\pi y \sqrt{1+\left[\frac{dy}{dx}\right]^2}\, dx$ $= \pi b \left[b + \frac{a^2}{\sqrt{a^2-b^2}} \sin^{-1} \frac{\sqrt{a^2-b^2}}{a^2} \right] dx$
$V_2 = \pi \int_0^{1.404a} b^2 - \frac{x^2 b^2}{a^2} dx = 0.943\pi ab^2$	$S_2 = \int_0^{1.404a} 2\pi y \sqrt{1+\left[\frac{dy}{dx}\right]^2}\, dx$ $= \pi b \left[0.702\sqrt{0.058a^2+1.971b^2} + \frac{2a^2}{\sqrt{2a^2-b^2}} \sin^{-1} \frac{1.404\sqrt{2a^2-b^2}}{2a} \right]$
$V_T = V_1 + V_2 = 1.609\pi ab^2$	$S_T = S_1 + S_2$

After the final fabrication was completed, the inspection revealed the following measurements: a = 0.7 m, b = 0.53 m, and l = 2.4a = 1.7 m.

5.1 Fabrication of the Final blimp body:

The final fabrication is done according to the calculation. Mylar and re-enforced polyester films are used to fabricate the blimp envelope.

Mylar polymer

The blimp envelope is made of Mylar polymer film shown in Fig. 5. Mylar is a commercial name of BoPET (biaxially oriented polyethylene terephthalate) which is a polyester type film made from stretched (PET). It is commercially used as packaging material, covering over paper, nitrogen-based food packaging, roasting bag, insulating material.

Fig. 5. The blimp envelope, made from Mylar polymer film

For outdoor use there is a problem with UV ray or over heat due to sun light. So, in that case silvering from the inside surface of the blimp body can give a perfect solution which is followed while the envelope is fabricated.

Table 2: Mechanical Property of Mylar

Mechanical Property	**Unit**	**Mylar**											
Total thickness	µm	19	23	36	50	75	100	125	190	250	300	350	500
Tensile strength	N/mm^2	210	210	230	190	190	190	180	190	190	190	190	150
Tensile strength	N/mm^2	230	230	260	210	200	200	200	220	200	200	190	170
Elongation at break longitudinal	%	110	130	130	140	140	150	150	190	210	210	240	270
Elongation at break	%	110	110	110	120	120	120	130	140	170	180	200	240
Shrinkage (30 min at 150 °C)	%	1,3	1,3	2	1,2	1,1	1,1	1,1	1,3	1,3	1,3	1,3	0,9
Shrinkage (30 min at 150 °C)	%	1	1	1,7	1,1	1	1	1	1,3	1,3	1,3	1,3	0,9
Shrinkage (30 min at 200 °C)	%	4	4	7	2,8	2,5	2,5	2,5	3,5	3,5	3,5	3,5	2,0
Shrinkage (30 min at 200 °C)	%	3	3	6,5	2,5	2,3	2,3	2,3	3,3	3,3	3,5	3,3	1,7

The mechanical property of Mylar is depicted in Table 2. The thickness of the Mylar films ranges from 19 µm to 500 µm, catering to various applications for their various range of strength, durability, flexibility. The tensile strength of mylar along the longitudinal direction is varied from

5 N/mm^2 to 230 N/mm^2, with the thinner films performing highest strength (19 µm and 23 µm). With the transverse direction, the tensile strength also varies from 170N/mm^2 to 260 N/mm^2, following a similar trend. The elongation at break in the longitudinal direction is varied from 110% to 270% increasing thickness while on the other hand in transverse direction the change would be from 110% to 240%. At different temperature this material has little change of its shape unto 6.5% increase. Despite having some robustness, it has some problem with ultra-violate rays and had effect upon the direct heat from sunlight in touch of UV. Silvering the inside portion of the mylar film would eventually reflect the sunlight from the surface and so it would have less effect of UV rays with direct heat from sunlight. So, silvering the inside surface of the mylar envelope during fabrication would eventually address the issue and reduce the absorption, and so the mylar envelope would gain a durable performance in outdoor application.

Re-enforced Polyethylene:

Fig. 6. The blimp envelope, made from re-enforced polyethylene

In case of re-enforced polyethylene shown in Fig. 6, the big advantages are its strength. For indoor use there are chances of being resisted by various object which can eventually results in failure. So, re-enforced blimp is a good material body for indoor use. As indoor capacity does not have any possibility to be in touch of UV ray or heat from sun. So, no silvering is needed. Reinforced polyethylene RPE is being explored as a promising material for indoor blimp material for its perfect strength. Mylar, a commonly used blimp material might be affected and tear down by indoor and outdoor obstacle. But on the other hand, RPE has a low specific gravity 0.07 for good buoyancy and it can prevent heat built up. Along with its capability of impressing tensile strength 117 MPa to resisting pulling force s and flexural strength of 186 MPa to handle bending force.

Considering the both cases, both the envelop were used for their buoyancy test. Hydrogen is used for final experiment as hydrogen has much more buoyant force than the helium.

6.0 Control system

According the dynamic modeling of the blimp system, the final output of the control system was fabricated with two kinds of motor. Both DC motor and BLDC motor are used. But it has been observed that BLDC motor served much better in outdoor with the proposed LQR based control system. From the below figure, it has been shown that, how the propulsion system would work for various movements.

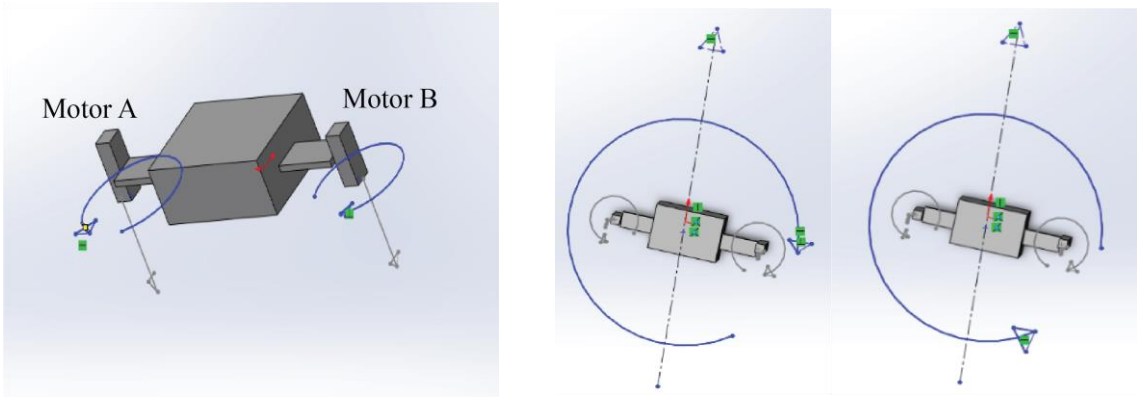

(a) (b)

Fig. 7. (a) The rotation direction of Motors A and B (b) Rotation of the blimp body with respect to Z axis due to differential speed of Motor A and B

Fig. 7. explains how the final control system output would work. A and B are the two-output motor which are responsible to give propulsion of the blimp system according to the desired required torque and rotation. The total momentum from both A and B motor, the final momentum would affect the system according to the control dynamics.

6.1 Control System Fabrication

Control system fabrication has been divided into two parts, one is for indoor blimp system and another is for outdoor blimp control system. For outdoor experiment BLDC motor has been used considering the requirement of higher controllability. DC motor with low rpm has been used for indoor control system development.

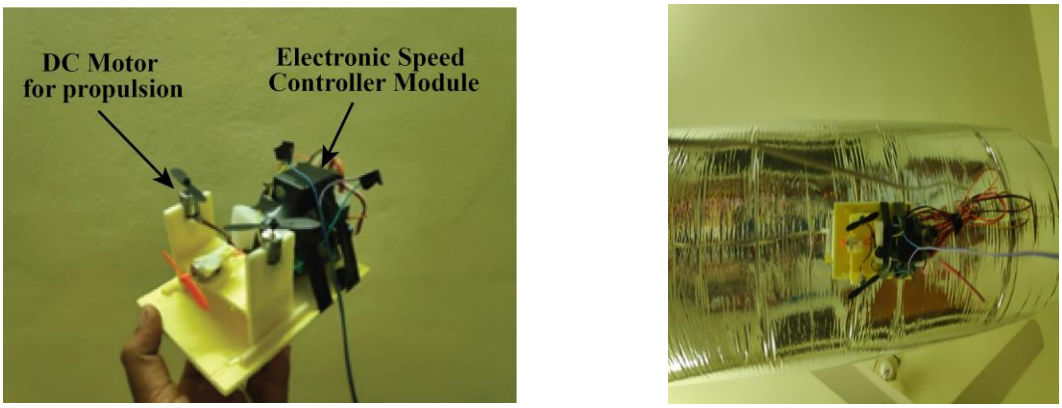

(a) (b)

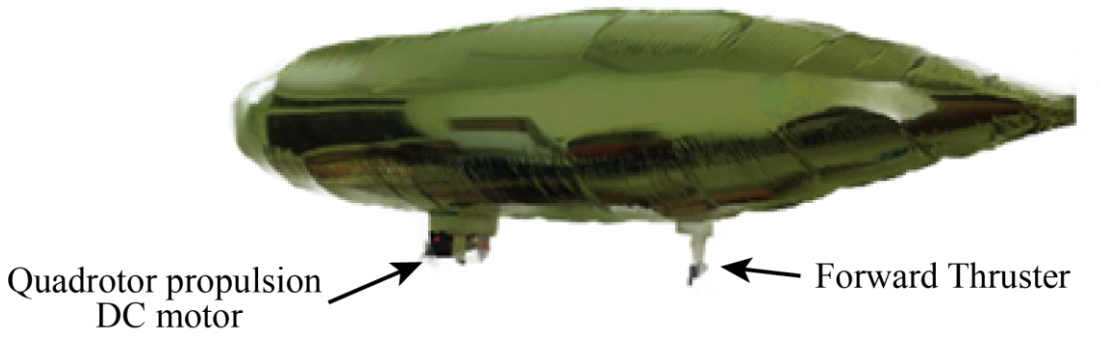

(c)

Fig. 8. (a) the control system for indoor blimp (b) bottom view of the blimp in indoor flight (c) Propulsion system of the blimp

Fig. 8. shows the final fabrication of the proposed LTA system with Mylar envelope, silvering on the surface of inner side and as a LTA gas Hydrogen has been used. But for propulsion system, 5V DC motor with 1500 rpm has been used. For indoor use, DC motor can serve the purpose as it has low RPM compare to the BLDC motor. For trial bases, the attachment platform between motor and blimp, some low-density light weight Depron sheet was used and here the 5th propulsion unit is signifying its position at the tail part of the blimp. So, using LQR controller and DC motor as controller final output, this setup is okay for indoor purpose. But, for outdoor controllability, it become harder while performing flight test.

Total five BLDC motor has been used for the final fabrication of outdoor blimp. As, very few work with this Penta rotor concept with LQR controller for a small blimp has been found from the previous work. Among the five BLDC motor, four of them were arranged in quadrotor X orientation and 5th BLDC motor has been placed at the back side at 90-degree rotation of back-thrust according to the dynamic modeling diagram, shown in Fig. 9(c). The main objective of the fifth BLDC motor would be to generate forward moving thrust force to the system. All the mountings of the BLDC motor have been fabricated with supporting platform made from Styrofoam.

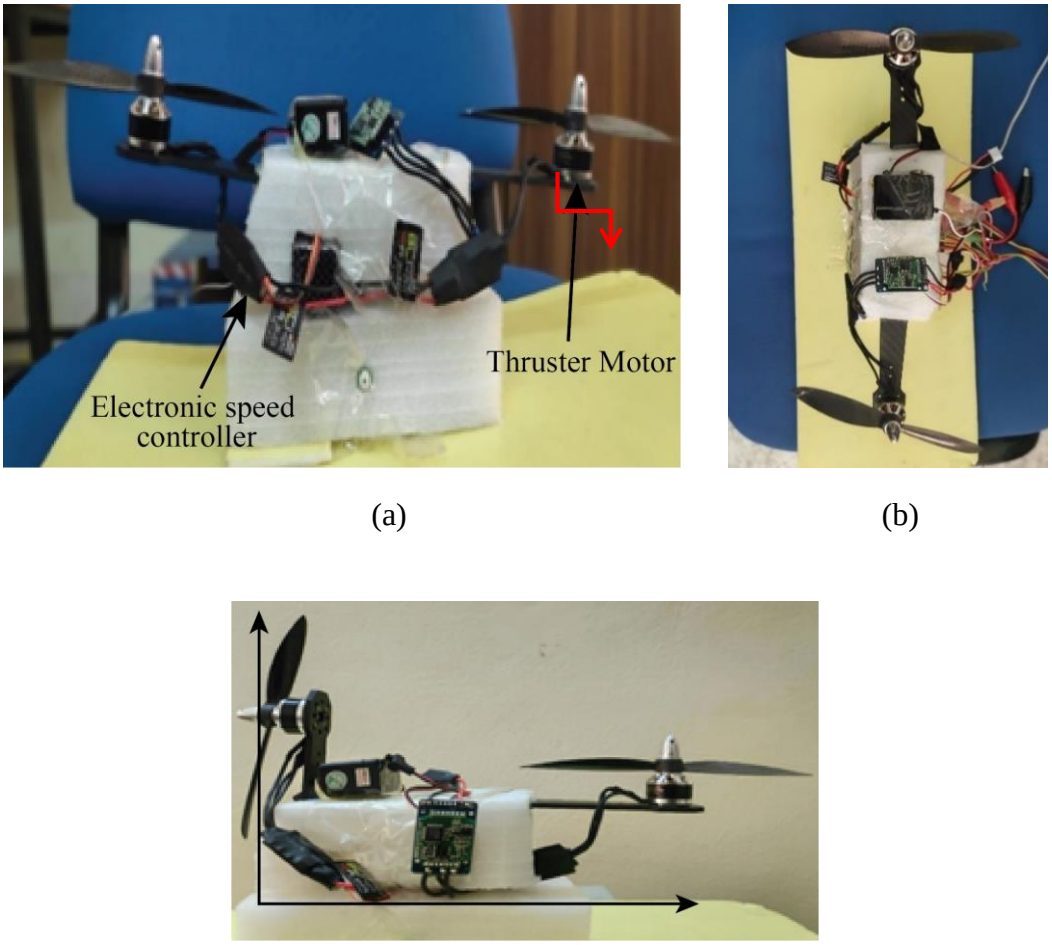

Fig. 9. (a) front & (b) top view of the differential propulsion system setup, (c) position of the forward thruster with respect to differential propulsion system

Final fabrication and control system setup has been done according to the Fig. 10. Raspberry pi controller has been used for executing LQR controller that we've designed. The control matrix would receive the input command from both radio controller or the computer command through open-source cloud. While receiving the command, the LQR controller would react by considering the command as target point and considering the difference between present and target point as error. A GPS tracking system along with internet modem would pass the signal through cloud. The blimp would provide the buoyancy force that support the system in flight time elongation. As, lithium polymer was the main power source, all the system power will receive the stored energy from battery. For the system, more weight means more thrust needed to keep the system on air. More trust leads to more energy consumption and create less flight time. Adding the blimp with would make the flight time long make the system sustainable for data monitoring.

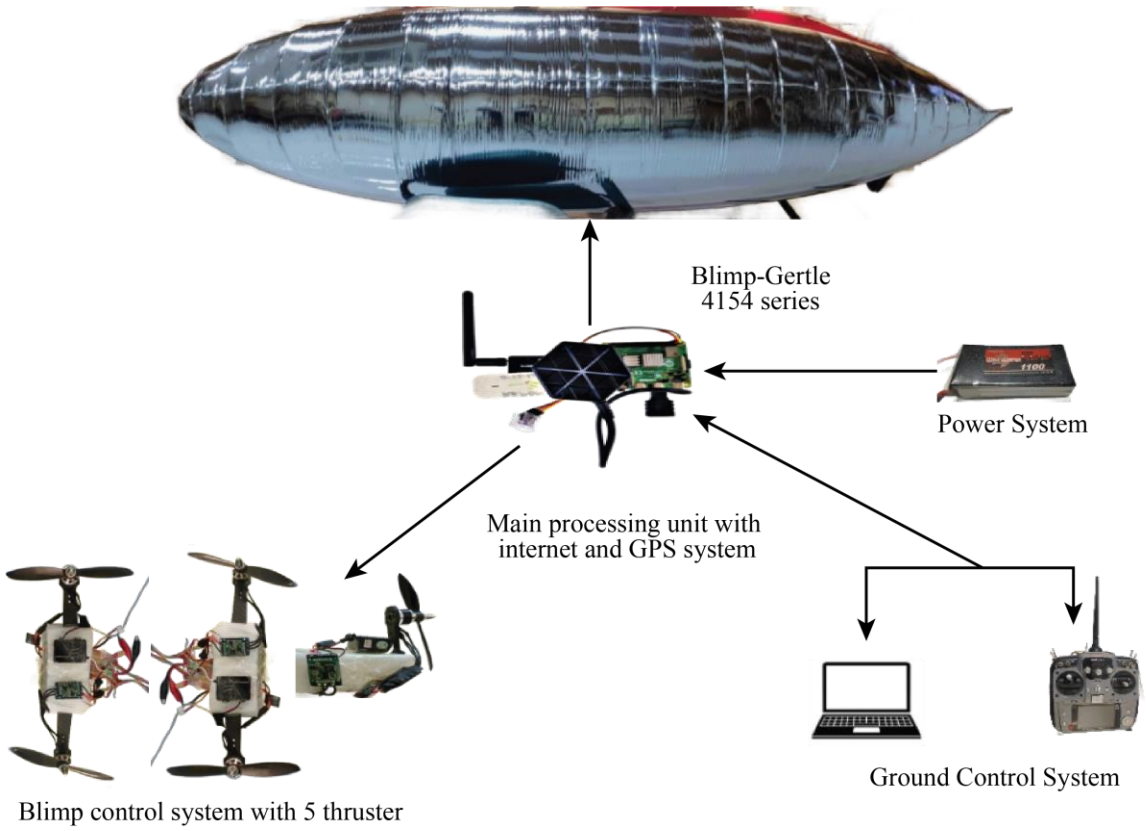

Fig. 10. Diagram of the control system of the penta-copter blimp

7.0 Result

For the selection of envelope, both the envelope with Mylar and re-enforced polymer were tested with hydrogen as a LTA gas. In the experiment, the envelope was infilled with hydrogen gas at the same time, the buoyancy force was measured with weight cell. Due to fabrication mistake, not sealing the inlet valve properly or impurity of the hydrogen gas would lead to the loose of buoyancy force. In this case, Mylar performed better result than re-enforced polymer.

This test has been carried out for 225 hr. and during the test shown in Fig. 11, a load cell was used for measuring the buoyancy force for both the envelope. At first, the bouncy force generated by re-enforced envelope was 195 gm and for Mylar it was 200gm. Though, the test was conducted it thus initial condition, the envelope can generate 250gm lift force at its highest Hydrogen intake condition. Over the time hydrogen gas has sacrificed its buoyancy force. But, after 150 hr. both the envelope losses their buoyancy force rapidly and at the end of the experiment re-enforced envelope and Mylar envelope contain nearly 140gm lift force at the end of 225hr. so, both the envelope would provide a sustainable lift force ranging from 250 to 140 for up to 225hr. use cycle. As this experiment was carried out at 25-degree room temperature and ground level atmospheric pressure, this result can be varying according to the altitude change

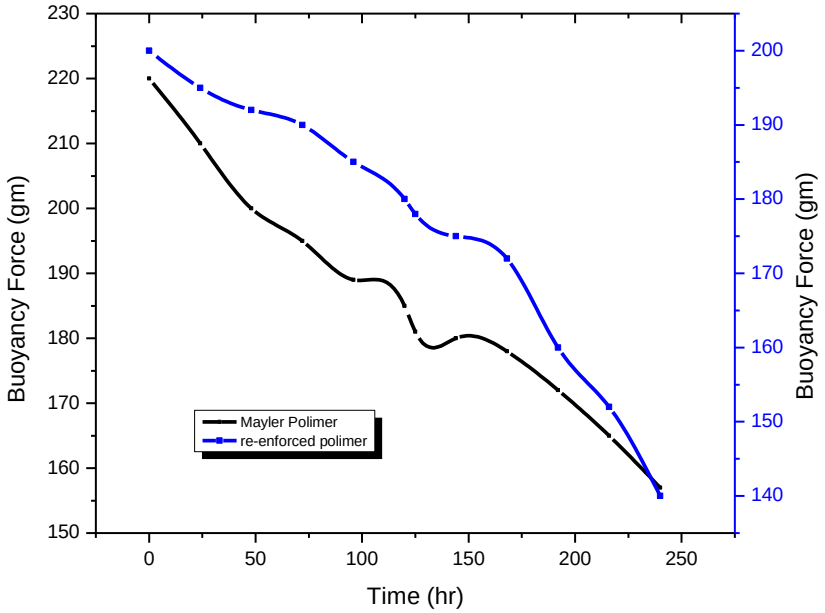

Fig. 11: Buoyancy gas performance during long time flight condition

After selecting the Mylar envelope for final fabrication, the thermal stability of the envelope material has been experimented through TG/DTA machine

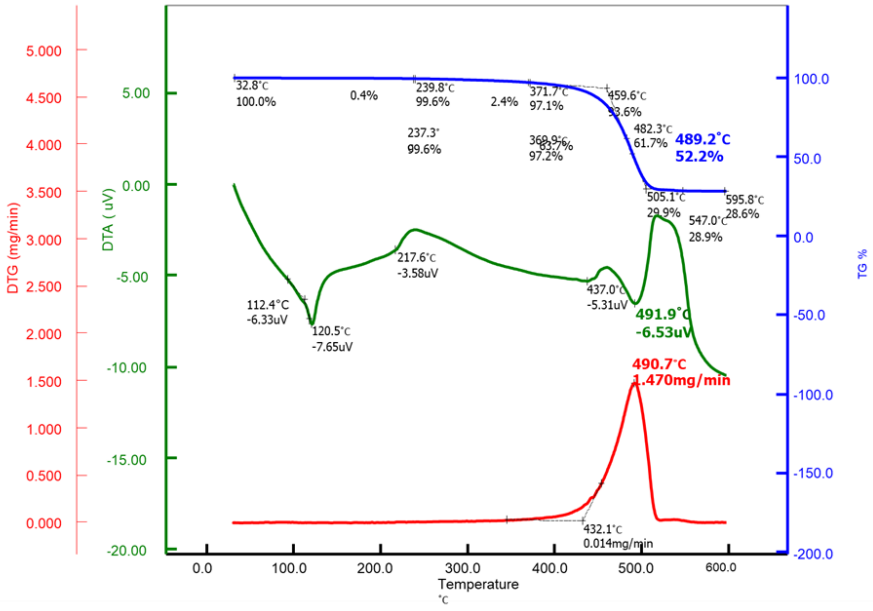

Fig. 12. TG, DTA, DTG plot with respect to temperature.

Fig. 12 shows the thermal stability of Mylar from room temperature 25 degree to 600 degrees [Sample Weight: 4.752 mg Reference Name: Aluminum, Reference Weight: 0.000 mg]. From the previous result of bouncy force, it has been found that mylar has better performance as n blimp envelope. So, Mylar was selected as a primary material and experimental envelope for the desired

control system. At 459-degree conscious temperature the envelope material started to deform. So, Mylar performed great in thermal stability.

7.1 Simulation of the control system using LQR controller

This part uses MATLAB to simulate the developed model. The blimp's location (X, Y, and Z) and orientation (yaw ψ) are determined from the findings. To achieve the desired locations (X, Y and Z), the regulated input vector u creates the roll(ϕ) and pitch(θ) that are required. Table 2 contains the values for the simulation's parameters.

Table 2. Parameters for MATLAB simulation.

Symbol	Definition	Value
FB	Buoyancy force	0.25kg
M	Mass of the system	0.3kg
m	Net mass of the Blimp	0.05 kg
g	Acceleration due to gravity	9.81 m/s²
r_1	Distance from the center to the motor (radius) along the x-axis	0.25 m
r_2	Distance from the center to the motor (radius) along the y-axis	0.25 m
l_x	Distance from the center of mass to each motor along the x-axis	0.0196 m
l_y	Distance from the center of mass to each motor along the y-axis	0.0196 m
l_z	Distance from the center of mass to each motor along the z-axis	0.0264 m
c	Constant	0.1

7.2 Response comparison with respect to different time

Controlling the blimp's location and orientations, i.e. X, Y, Z, and ϕ, is the goal. The following are the desired values of the parameters for the blimp's-controlled position: Z = 11 m, X = 6m, Y = 8m, and ψ = 0 rad. Less than 2s of rise time is ideal for the blimp to reach its target places. With a LQR-based controller, the following outcomes are obtained.

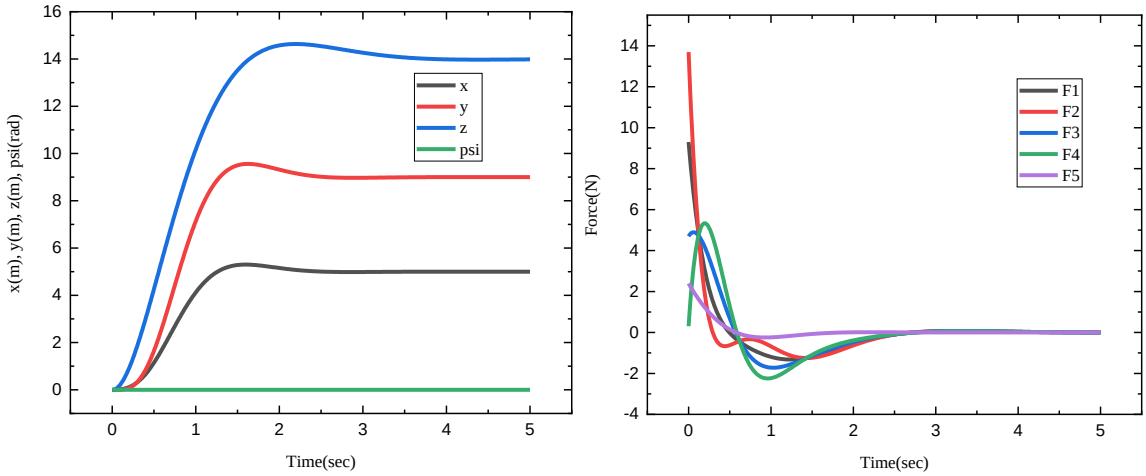

(a) (b)

Fig. 13. (a) Behavior of the blimp (b) Forces required to stabilize the system

The blimp obtained desired X, Y position and psi orientation within ~3 second shown in Fig. 13. But Z position takes a large amount of time of ~4s to settle in a stable state which is not desirable. The problem can be solved by increasing the corresponding element in the Q matrix. The (3,3) element is responsible for Z response in this system. The modified matrix became, $Q = diag([8,\ 3,\ 5,\ 0,\ 0,\ 0,\ 1,\ 1,\ 1,\ 0,\ 0,\ 0])$. In Fig. 14 the settling time for Z is ~2.5sec. The required force for settling in Z position is shown in Fig. 14. Comparing the forces with Fig. 13, it can be clearly seen that, the forces are increased after modifying the Q matrix to achieve a faster response for Z position.

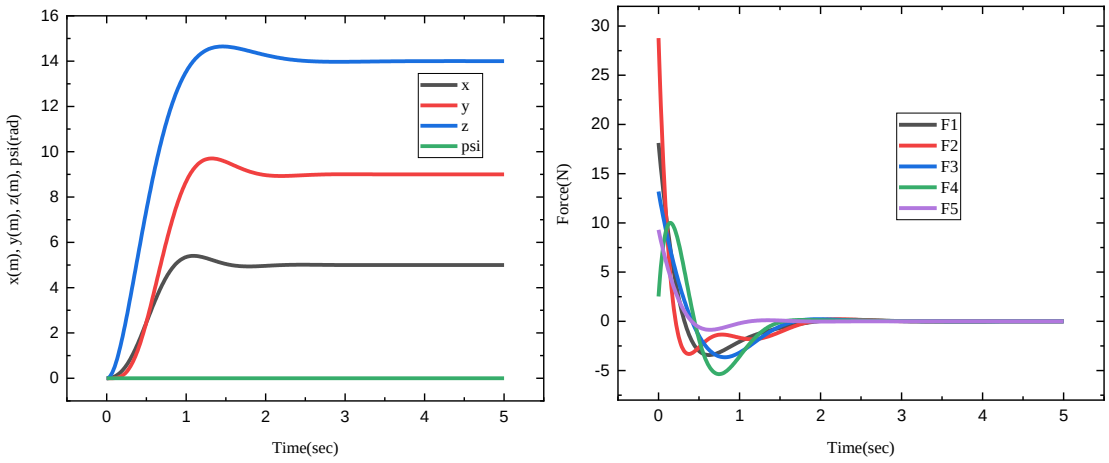

(a) (b)

Fig. 14. (a) Behavior of the blimp (b) Forces required to stabilize the system after changing the Q matrix

7.3 Trajectory Planning and Actuator response- Different coordinate

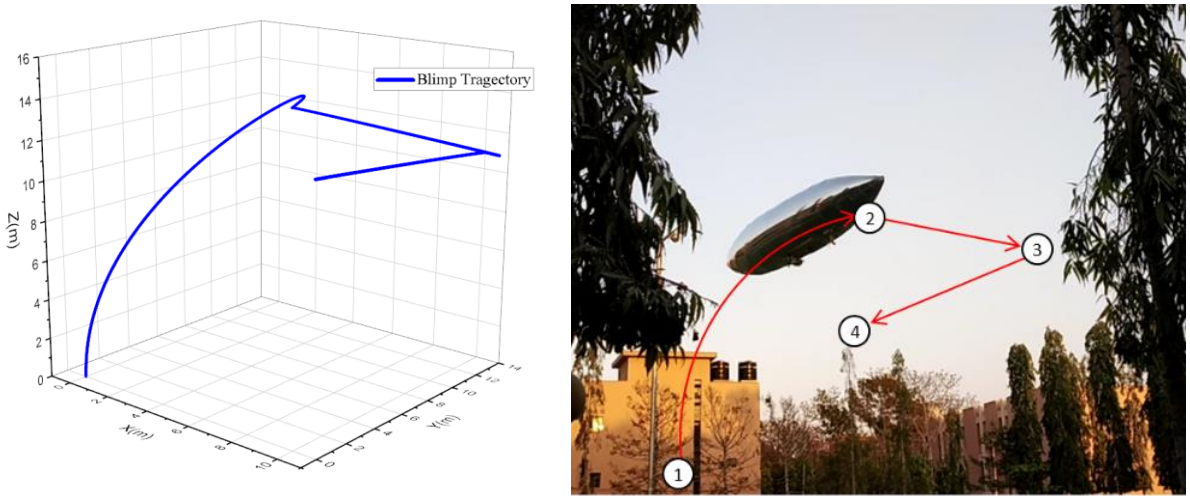

(a) (b)

Fig. 15. Simulated and experimental trajectory of the Blimp

Fig. 15. shows the trajectory followed by the blimp from a given desired way points in the simulation. The way points are given as (0, 0, 0), (2, 12, 12), (12, 10, 12), (10, 2, 12). The behavior of the blimp and the forces required to achieve the stability of the system is shown in Fig. 16. and Fig. 17. respectively. Trajectory planning is an important part for any kind of system. For the study a preset trajectory was designed for finding the response of the actuators or BLDC motors. But generally, from radio control command or GPS based point to point command provide a directional motive for a specific trajectory planning. Introducing computer vision or LIDAR based sensor system could help the trajectory planning for avoiding obstacles. Just to verify the system with LQR controller, a sample trajectory was introduced according to the Fig. 15(a), practical flight test has been done in open filed shown in Fig. 15(b). Due to wind and other factors, the final test was far different than the trajectory planning.

For the trajectory planning that have been done during the test flight and shown in Fig. 15, state variables were changed according to the trajectory which is shown in figure 16. Position change along X, Y, Z, velocity along the axis's denoted as X_vel, Y_vel, Z_vel. For rotational movement, roll, pitch, yaw and their rotational velocity

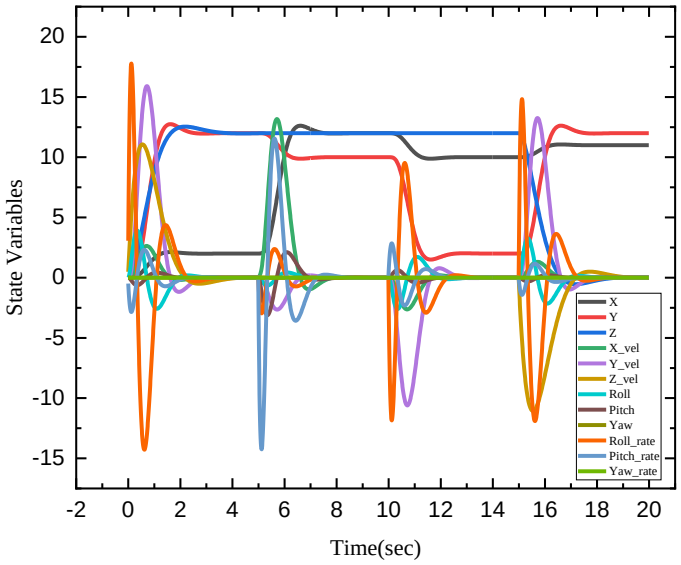

Fig. 16. Behavior of the blimp during the simulation

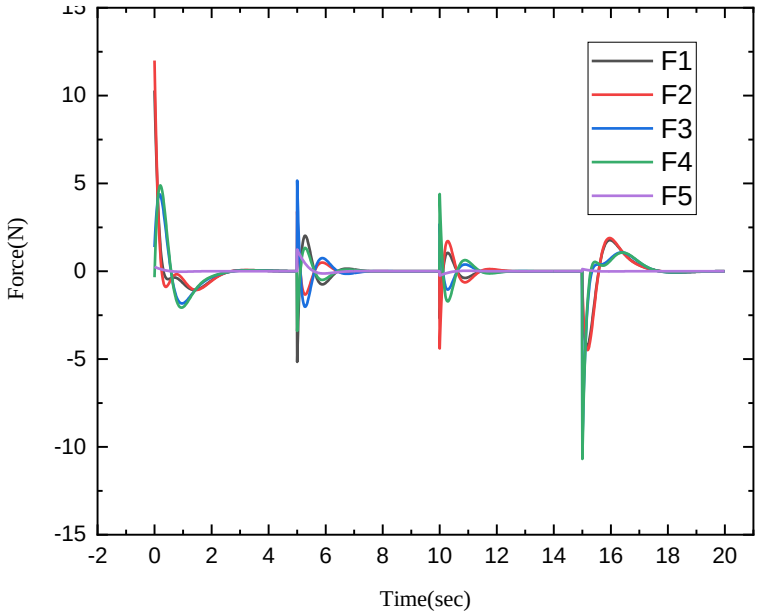

Fig. 17. Forces acting on the blimp during the simulation

For obtaining the state variable changes over time according to the trajectory planning the propulsion system has to generate force. As, the proposed system, has five propulsion system Fig. 17 shows the fluctuation in force generating BLDC motors total generated force over flight time.

Simplified Trajectory planning in different points node has been shown in Fig. 18. According to the trajectory planning its simplified version of state variable has shown the clear picture about the system response. Fig. 18. shows the trajectory followed by the blimp from a given desired way points in the simulation. The way points are given as (0, 0, 0), (0, 15, 12), (10, 15, 15), (15, 12,

15), (15, 3, 0). The behavior of the blimp and the forces required to achieve the stability of the system is shown in Fig. 16 and Fig. 17 respectively.

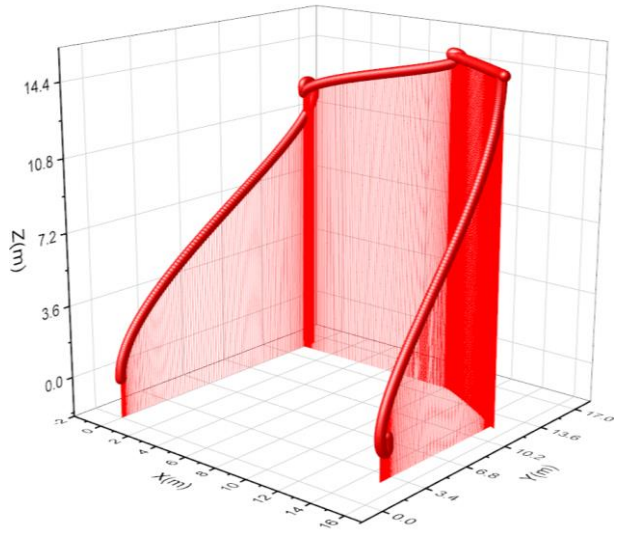

Fig.18. Simulated trajectory of the Blimp

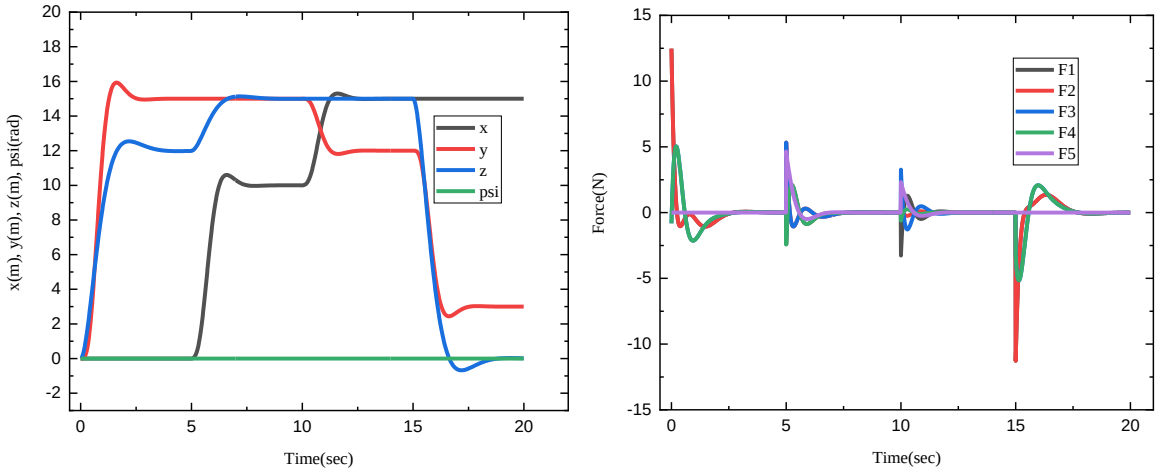

Fig. 19. (a) Behavior of the blimp (b) Forces required to stabilize the system

(a) Stable Condition

(b) Forward approach

(c) Rotational movement

(d) Farther rotational movement

(e) New directional movement

(f) Forward movement to new direction

Fig. 21. Final experimental flight test of the Blimp using penta-rotor trust system with LQR based controller

7.4. Effective Power management

LTA technology in aerial robotics field is an old concept in new dimension. LTA technology has concentrated objective of long-time flight as its LTA gas provide the lift. The control system would only work on the mobility of the body. While using traditional or manual control system, the power management would be functioned accordingly. But in LQR controller, there would be an easy power management constant that signifies which motor would be functioned more in which command or state variable. Fig. 20. shows the trajectory that would be followed by the system for the test. There would be their node point for state variable (0, 0, 0), (0, 0, 12), (10, 0, 12). While it gets the command for (0, 0, 12) to (10, 0, 12), it has a forward error from 0 to 10 meter along X axis. So, it would generate a forward thrust with differentiation motor rpm. in Fig. 21(a), in 5 sec time F1 to F4 works as a traditional quadrotor configuration for provide the vehicle a forward

thrust. But, while the LQR constant has been changed, we can have a clear difference from Fig. 21(b) with the same trajectory.

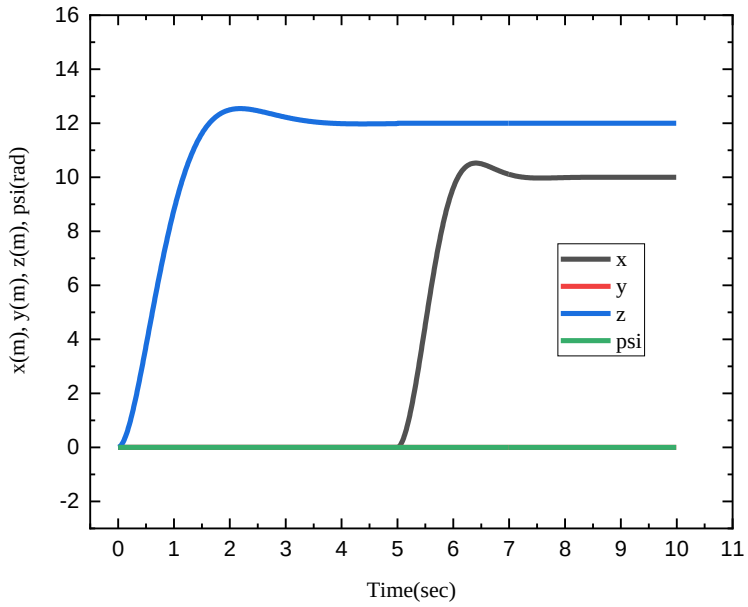

Fig. 20. Trajectory plot for the blimp system

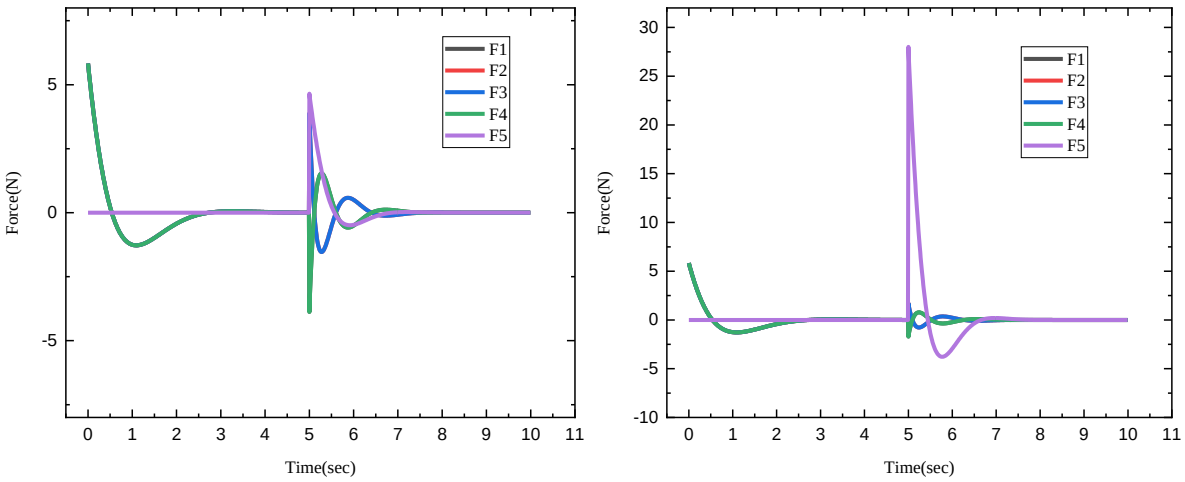

Fig. 21. Biased power consumption for energy efficiency

In Fig. 21(b), using same trajectory but different control constant Q, response of F5 make a difference in power consumption with compare to other propulsion systems from F1 to F4. The blue line from Fig. 21(b) shows that, F5 had aggressive response at 5 sec flight time while changing its position from (0, 0, 12) to (10, 0, 12). As for forward movement, it needed forward thrust. For forward thrust, there are two possibilities for mobility generation. One in the active participation of all motors from F1 to F5 and another is aggressive participation of F5 and other F1 to F4 for

keeping the balance. With LQR controller it can be easily objectified that, as second possibility makes the system power efficient the possibility can be executed while there are commands through state variable to move forward along X axis.

8.0 Discussion:

On this work, the performance of a LTA drone was significantly increased by integrating dynamic modeling, propulsion system analysis and an LQR-based control system. The dynamic modeling step successfully captured the complex interaction between buoyancy forces and aerodynamic force effect, this leading to an enhanced representation of the blimps motion in various operational condition. By including these forces into the equation of motion, the study was able to provide the drones behavior with greater accuracy, stability and improved control. On the other hand, the analysis of the propulsion system propulsion system came with some valuable insights into important parameters influencing system efficiency and allowing better optimization of power consumption and motor performance combined with advance modeling with the help of force distribution in stabilizing the blimp during flight.
The integration of LQR based control mechanism proved instrumental ability to make the system more stable not in physically but in power management system in various controlled state variables through trajectory. Simulation results show that, by adjusting the element of the Q matrix, the respond time of the blimp would significantly improve. Particularly in the vertical axis (Z), where modifications led to faster settling times without compromising stability. This indicates that the system is highly tunable and adaptable to specific operational requirements.

Trajectory planning, both in simulation and practical flight test express the robustness of the control system. In spite of the challenges such as environmental factors, the system shows a consistent and reliable flight performance. The inclusion of LQR based controller adjustment in the propulsion system through BLDC motor demonstrate the optimized power consumption. This is very much significant in achieving extended flight durations which is the most primary objective for LTA blimp.

In the work some valuable finding suggests that introducing advance control systems like LQR with trajectory planning method would lead a way for more advanced and autonomous and energy efficient blimp operations, especially when thus control system and dynamic framework would be attached with some advance sensor modules like computer vision or LIDAR for obstacle avoidance. Thus, sensor input would lead to the state variables and final mobility would be executed through the LQR controller in a very energy efficient way. Overall, the synergy between dynamic modeling, propulsion system analysis and control optimization has provided a viable solution for long-duration and energy efficient autonomous flight.

9.0 Conclusion

In conclusion, this paper has undertaken a comprehensive exploration into enhancing the performance of a LTA aerial drone through dynamic modeling, propulsion system analysis, and the integration of an LQR-based control system. The dynamic modeling section meticulously examines the drone's equations of motion, incorporating aerodynamic and buoyancy forces to accurately depict its behavior across diverse operational scenarios. Furthermore, the propulsion system analysis delves into modeling techniques for the chosen propulsion system, identifying critical parameters influencing its efficiency. By integrating an LQR-based control system, the paper elucidates the principles and advantages associated with its application in aerial drones. Through simulation and analysis, valuable insights are provided into the synergistic effects of dynamic modeling, propulsion system characteristics, and LQR-based control on overall drone performance. The results of the simulation analysis underscore the efficacy of the developed controller, emphasizing its potential to optimize design considerations and operational capabilities. This integrated approach signifies a significant stride in advancing the capabilities of aerial drone technology, with the detailed Blimp dynamics model and the application of LQR-based control marking notable contributions to the field.

Reference

[1] P. Herman, "Various Control Strategies," in *Springer Tracts in Mechanical Engineering*, 2022. doi: 10.1007/978-3-030-94647-0_5.

[2] T. Yamasaki, H. Fujita, and N. Goto, "Identification of blimp dynamics by indoor free flight tests," in *AIAA Atmospheric Flight Mechanics Conference and Exhibit*, 2002. doi: 10.2514/6.2002-4405.

[3] H. Furukawa and A. Shimada, "Wind-disturbance-based control approach for blimp robots," *Electron. Commun. Japan*, vol. 97, no. 2, 2014, doi: 10.1002/ecj.11498.

[4] S. Yu, P. Yu, and T. Tang, "Effect of thermal buoyancy on flow and heat transfer around a permeable circular cylinder with internal heat generation," *Int. J. Heat Mass Transf.*, vol. 126, 2018, doi: 10.1016/j.ijheatmasstransfer.2018.06.056.

[5] Y. Bestaoui and H. Kuhlmann, "A Newton Euler approach to modeling of a quad-rotor autonomous airship - Preliminary results," in *48th AIAA Aerospace Sciences Meeting Including the New Horizons Forum and Aerospace Exposition*, 2010. doi: 10.2514/6.2010-39.

[6] T. Takaya, H. Kawamura, Y. Minagawa, M. Yamamoto, and A. Ouchi, "Motion control in three dimensional round system of blimp robot," in *2006 SICE-ICASE International Joint Conference*, 2006. doi: 10.1109/SICE.2006.315440.

[7] T. Stachiw, A. Crain, and J. Ricciardi, “A physics-based neural network for flight dynamics modelling and simulation,” *Adv. Model. Simul. Eng. Sci.*, vol. 9, no. 1, 2022, doi: 10.1186/s40323-022-00227-7.

[8] N. M. Zaber, A. J. Ishak, A. C. Soh, M. K. Hassan, and Z. Z. Abidin, “Designing PID controller for position control with disturbance,” in *I4CT 2015 - 2015 2nd International Conference on Computer, Communications, and Control Technology, Art Proceeding*, 2015. doi: 10.1109/I4CT.2015.7219607.

[9] H. Kawamura, H. Kadota, M. Yamamoto, T. Takaya, and A. Ohuchi, “Motion Design for Indoor Blimp Robot with PID Controller,” *J. Robot. Mechatronics*, vol. 17, no. 5, 2005, doi: 10.20965/jrm.2005.p0500.

[10] D. S. Lee *et al.*, “The contribution of global aviation to anthropogenic climate forcing for 2000 to 2018,” *Atmos. Environ.*, vol. 244, 2021, doi: 10.1016/j.atmosenv.2020.117834.

[11] L. M. Argentim, W. C. Rezende, P. E. Santos, and R. A. Aguiar, “PID, LQR and LQR-PID on a quadcopter platform,” in *2013 International Conference on Informatics, Electronics and Vision, ICIEV 2013*, 2013. doi: 10.1109/ICIEV.2013.6572698.

[12] F. Ahmad, P. Kumar, A. Bhandari, and P. P. Patil, “Simulation of the Quadcopter Dynamics with LQR based Control,” in *Materials Today: Proceedings*, 2020. doi: 10.1016/j.matpr.2020.04.282.

[13] M. E. C. Funez, A. F. B. Aponte, S. P. Triana, L. C. R. Barrios, D. V. Munoz, and P. A. M. Tamayo, “A PID-controlled quadcopter system: The effect of parameters selection,” in *2020 9th International Congress of Mechatronics Engineering and Automation, CIIMA 2020 - Conference Proceedings*, 2020. doi: 10.1109/CIIMA50553.2020.9290298.